Part III Project: Late Time Constraints on Decaying Dark Matter

Author: Calvin Preston

College: Robinson

Supervisor: Professor George Efstathiou

Abstract

This project first investigates the claim made by Vattis, Koushiappas, and Loeb (2019) that decaying dark matter might provide a solution to the H_0 tension. We do this by reconstructing the expansion history of a universe with decaying dark matter and comparing to 1a supernovae and baryon acoustic oscillation data. We then constrain cosmological parameters using a Markov chain Monte Carlo analysis and inverse distance ladder comprised of a range of cosmological data sets, concluding that decaying dark matter does not offer a solution to the tension. By then investigating the fractional case, whereby only a fraction of the dark matter in the universe decays, we motivate an examination of the effect of decaying dark matter on structure formation. This leads to an investigation into the effect of decaying dark matter on the σ_8 and S_8 tensions. We see that it may offer a solution, but it is not fully satisfactory. The evolution of the overdensity field with redshift is then investigated, showing how decays affect the linear growth rates. Finally, we discuss how decaying dark matter may be realised in string theory, via the coupling of a light scalar field to dark matter. Our work could be extended to investigate such models.

Contents

1. Introduction . . . 2
2. Tensions in Modern Cosmology Explained . . . 3
   2.1 - The H_0 Tension and its Possible Solutions . . . 3
   2.2 - The σ_8/S_8 Tensions . . . 5
3. The Equations, Properties and Amount of Decaying Dark Matter . . . 6
   3.1 - The Properties of our Decay Products . . . 6
   3.2 - Initial Conditions Set on Decaying Dark Matter . . . 7
4. What To Expect in the Decaying Dark Matter Scenario . . . 8
   4.1 - The Expansion History of Various Universes . . . 8
   4.2 - Magnitude - Redshift Relations and Decaying Dark Matter . . . 9
5. The H_0 Tension Investigated in a Decaying Dark Matter Universe . . . 11
   5.1 - $\epsilon = 1$ . . . 11
   5.2 - $\epsilon \neq 1$ . . . 16
6. Structure Formation and the σ_8 and S_8 Tensions with Decaying Dark Matter . . . 17
   6.1 - The Evolution of the Linear Overdensity Field . . . 17
   6.2 - Structure Parameters at $z = 0$ . . . 18
   6.3 - Structure Parameters at $z \neq 0$ . . . 22
7. Realising Dark Matter Decays Via String Theory . . . 23
   7.1 - Rolling Scalar Fields . . . 23
   7.2 - What is the Distance Conjecture and What Can It Offer Us? . . . 23
   7.3 - Concluding Quintessence . . . 23
8. Conclusions . . . 24

Appendices **25**

Appendix A - Deriving the Conservation Equations of Decaying Dark Matter . . . 25
Appendix B - H_0 and H_0^S . . . 27

References **28**

1. Introduction

As is now well-established in the modern era of precision-cosmology, a six-parameter cold dark matter universe with positive cosmological constant Λ, the ΛCDM model, fits a range of cosmological datasets. This encompasses the temperature and polarization power spectra of the Cosmic Microwave Background (CMB) measured exquisitely by Planck (Planck collaboration et al. 2018) fitting a near-scale invariant spectrum of adiabatic Gaussian primordial fluctuations almost perfectly. However, in recent years, tensions between important cosmological parameters measured in different ways (specifically CMB measurements versus local supernovae measurements and large-scale structure surveys) have become apparent. The most famous of these is the "Hubble tension", regarding the 4.5σ difference between CMB and traditional distance ladder measurements of the Hubble parameter at $z = 0$, H_0 (Bernal, Verde, and Riess 2016; Di Valentino et al. 2021b). Also of interest are the σ_8 and S_8[1] tensions, parameters that measure the variance of the matter overdensity field in the universe (Di Valentino et al. 2021a).

As we do not understand the nature of Λ, nor the true identity of dark matter, there is scope for specific models of both Λ and dark matter to provide theoretical solutions to these cosmological tensions. In recent years these have come in a range of forms. The literature has seen discussion of non-ΛCDM models such as cannibal dark matter (Buen-Abad, Emami, and Schmaltz 2018), non-thermal dark matter (Alcaniz et al. 2021), dissipative dark matter (Silva, Gimenes, and Silva 2019), partially acoustic dark matter (Lin et al. 2019), self-interacting dark matter (Archidiacono et al. 2019) and, crucially for this project, decaying dark matter (Ichiki, Oguri, and Takahashi 2004; Audren et al. 2014; Vattis, Koushiappas, and Loeb 2019; Enqvist et al. 2020; Clark, Vattis, and Koushiappas 2021), henceforth DDM.

This project investigates the last of these models, motivated by the claims made by Vattis, Koushiappas, and Loeb (2019) that DDM can solve the H_0 tension. They conclude that DDM where the daughter particles are essentially massless and relativistic (some form of dark radiation), can alleviate the tension (this is discussed more in Section 2). This conclusion is in conflict with claims made by Efstathiou (2021), who argues that no late-time changes to ΛCDM can resolve the H_0 tension. By using an inverse distance ladder approach that places very tight constraints on cosmological parameters at late times, Efstathiou (2021) demonstrates the data does not allow for deviations from ΛCDM at the present epoch. The minimum aim of this project is to resolve this discrepancy, and then to further investigate the theoretical implications of DDM.

In section 3, we investigate the effect of DDM by first re-deriving the cosmological conservation equations including DDM. These are then used to reconstruct the expansion history ($H(z)$ as a function of redshift z) of the universe, observing deviations from ΛCDM in the presence of DDM in section 4.1. In section 4.2, we will then compare Ia Supernovae (SNIa) apparent magnitude data with what we expect from apparent magnitude-redshift relations in a universe with DDM. Then, we complete our analysis of the H_0 tension with DDM in section 5 by exploring the cosmological parameter space offered by DDM with a Markov chain Monte Carlo (henceforth MCMC) analysis. We follow the inverse distance ladder approach as in Efstathiou (2021), constraining our parameter space likelihoods with baryon acoustic oscillation, quasar, SNIa and Lyman-α absorber data.

We shall then investigate the effect of DDM on the growth of large-scale structure. We begin this by reconstructing linear growth curves in different DDM universes in Section 6.1. Then in Section 6.2 we examine how DDM can positively effect (though not conclusively solve) the σ_8 and S_8 tensions, and how it compares with weak lensing data from the Kilo-Degree Survey (KiDS) team's most recent work (Heymans et al. 2021). In Section 6.3 we investigate how DDM affects the growth of linear fluctuations as a function of redshift z. Finally, in section 7 we review a well-motivated model of DDM that is a consequence of string theory. Specifically we review the 'distance conjecture', and how the coupling of a light scalar field to dark matter can provide a realisation to our dark matter decays (Agrawal, Obied, and Vafa 2021). We conclude the investigation in Section 8.

[1] These parameters are defined and described fully in Section 2.2

2. Tensions in Modern Cosmology Explained

Before we begin investigating DDM, it is important to further understand the motivation for this project. These motivations are the cosmological "tensions" seen at present day. These are outlined, along with solutions currently being investigated, below.

2.1 - The H_0 Tension and its Possible Solutions

The Hubble, H_0, tension is the $> 4\sigma$ difference between the value of the Hubble parameter at $z = 0$ when measured in two different ways. The parameter H_0 measures the expansion rate of the universe at present day (Weinberg 2008). The Planck team report a value of $H_0^P = 67.4 \pm 0.5$ kms^{-1}Mpc^{-1} (Planck collaboration et al. 2018). The SH0ES [2] team most recently reported a value of $H_0^S = 73.2 \pm 1.3$ kms^{-1}Mpc^{-1} (Riess et al. 2021). The methodologies of the two teams are summarised below.

The SH0ES team measure H_0 by building a conventional cosmological distance ladder as follows: The luminosity-period relation of variable classical Cepheids (massive stars that lie on the instability strip of the Hertzsprung-Russell diagram) are observed in very nearby systems. These stars can then be used as standard candles. They become an anchor for calibration of the luminosity distance to more distance Cepheid stars in systems that host SNIa (the thermonuclear explosion of a white dwarf star having exceeded its Chandrasekhar mass limit). This then provides an absolute calibration for the SNIa magnitude-redshift relation that one can then match to the Hubble flow, giving a determination of the Hubble parameter via local measures (with sources at a redshift no more than $z < 0.007$). The exact relation between luminosity distance and H_0 is discussed in more detail in Section 4.2 (Freedman 2021).

The Planck team take a very different approach. Using a satellite to collect primordial photons that still stream through our universe, they measure anisotropies in the temperature and polarisation of the photons of the CMB, released at redshift $z > 1000$. From this information, the acoustic peak in the temperature and polarisation power spectra constrain the value of H_0 under the assumption of a ΛCDM cosmology (Planck collaboration et al. 2018).

These results of the teams two values of H_0 do not agree with one another differing by 4.3σ (using Riess et al. (2021) most recent work), and hence are in a "tension" with one another (Bernal, Verde, and Riess 2016; Aylor et al. 2019; Di Valentino et al. 2021b). This tension is illustrated in Figure 1 below.

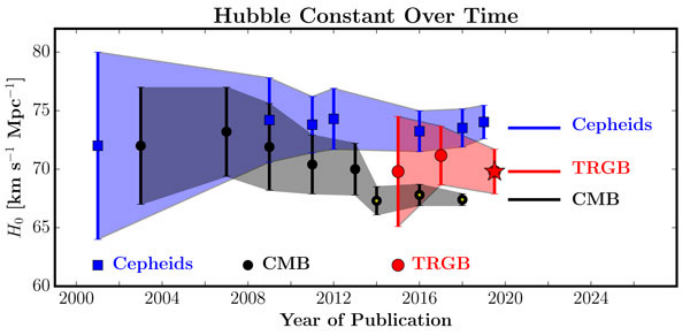

Figure 1: The H_0 tension visualised. Different measurements of the Hubble Constant, including more recent tip of the red giant branch measurements. Error bands correspond to 1σ errors. Image credit: Freedman (2021)

We see here the severity of the tension. It should be noted that more recent work with using the Tip of the Red Giant Branch (TRGB) approach reports a value $H_0 = 69.6 \pm 0.8$ kms^{-1}Mpc^{-1} (Freedman et al. 2020) using a method similar to that of SH0ES, but with the Carnegie Supernovae Project Data (Hamuy et al. 2006; Krisciunas et al. 2017) replacing the Pantheon Supernovae Data and using the TRGB as a standard candle instead of Cepheids. It is interesting to note how the value of H_0 from this method falls between the

[2] Supernovae, H_0, for the dark energy Equation of State

values from SH0ES and Planck.

There are a wide range of theoretical solutions suggested in the literature to resolve this tension, as well as claims of systematic errors unaccounted for in the geometrical distance ladder process (Efstathiou 2020; Rameez and Sarkar 2021) that will not be discussed here. Theoretical solutions to this tension generally fall into one (or more) of four main categories:

i) Departures from general relativity and a flat Friedman Robertson Walker universe

ii) Changes at early times (during inflation or pre-recombination physics)

iii) Physics to alter the value of the sound horizon

iv) Changes to late-time physics

We do not consider scenarios i) - iii) here. We restrict ourselves to iv), as it is within this class of solutions that Vattis, Koushiappas, and Loeb (2019) investigate DDM and claim that it can alleviate the H_0 tension.

For their work, they consider a decaying dark matter model where a massive parent particle ψ decays into two daughter particles, one massive and one massless (χ and ϕ respectively). This general decay scenario is of the form

$$\psi \rightarrow \chi + \phi \, .$$

They assume no decays have taken place before recombination, set at $z_{rec} = 1090$, and assume ΛCDM priors. Unless the masses of ψ and χ are nearly equal, χ will be highly relativistic and behave like radiation. To simplify our own analysis, we will assume that χ is effectively massless (this is discussed more in Section 3). As a result, their general argument is that decays can alter the redshift of matter-dark energy equality, and could bring $H(z)$ into agreement with measures at $z = 0$.

However, it is easy to see that this scenario is unlikely to solve the H_0 tension. We can see this from considering how both matter and radiation scale with redshift in a universe described by a Friedmann-Robertson-Walker (FRW) metric.

Matter density scales with redshift as $\rho_M \propto (1+z)^3$, whilst radiation density scales as $\rho_R \propto (1+z)^4$. If dark matter were to decay from a matter component (as standard cold dark matter belongs to the matter, Ω_m, density fraction parameter) to a radiation component, we should expect it to dilute faster with redshift as the universe evolves. As such, the energy density sum of matter and radiation at $z = 0$ will be smaller in a universe where decays have taken place due to this diluting effect, and so a Hubble parameter consisting of the sum of densities of all components at a given redshift will be of a lower value in the presence of DDM. As such, any decays of dark matter cannot alleviate the H_0 tension.

By introducing more parameters to their cosmological system of equations, Vattis, Koushiappas, and Loeb (2019) widen error bars in their expansion history such that Planck's and SH0ES' results marginally overlap. As we will show, this is not a fully satisfactory solution to the H_0 tension. The authors do not comment on the σ_8/S_8 tensions.

2.2 - The σ_8/S_8 Tensions

The S_8 tension is the approximately 3σ difference in the value of S_8 between measurements inferred from Planck observations of the CMB, (Planck collaboration et al. 2018), and various large-scale structure survey results (all of which report slightly different values for S_8, discussed in more details below). The cosmological parameter S_8 is defined as

$$S_8 = \sigma_8 \sqrt{\frac{\Omega_m}{0.3}} \, ,$$

where σ_8 is the variance of the matter over-density field measured in spheres of radius $8h^{-1}$Mpc and Ω_m is the density parameter of non-relativistic matter (with Planck value $\Omega_m = 0.3111 \pm 0.0056$ (Planck collaboration et al. 2018)).

For S_8, the Planck team report a value of $S_8 = 0.834 \pm 0.016$ (Planck collaboration et al. 2018), whilst the analysis of weak-lensing data by the Kilo-Degree Survery (KiDS-1000) team report a value of $S_8 = 0.766^{+0.020}_{-0.014}$ (Heymans et al. 2021).

For σ_8, the situation is similar. Planck report a value of $\sigma_8 = 0.8102 \pm 0.0060$, whilst KiDS report $\sigma_8 = 0.76^{+0.025}_{-0.020}$. These parameters are, again, not in good agreement with one another. The tension here is in the opposite ordering to that the H_0 tension, as for σ_8 the Planck value is larger than other measures, whilst for H_0 the Planck value is smaller than other measures. Planck predicts a less smooth, less rapidly expanding universe. The σ_8 tension is visualised in Figure 2 below

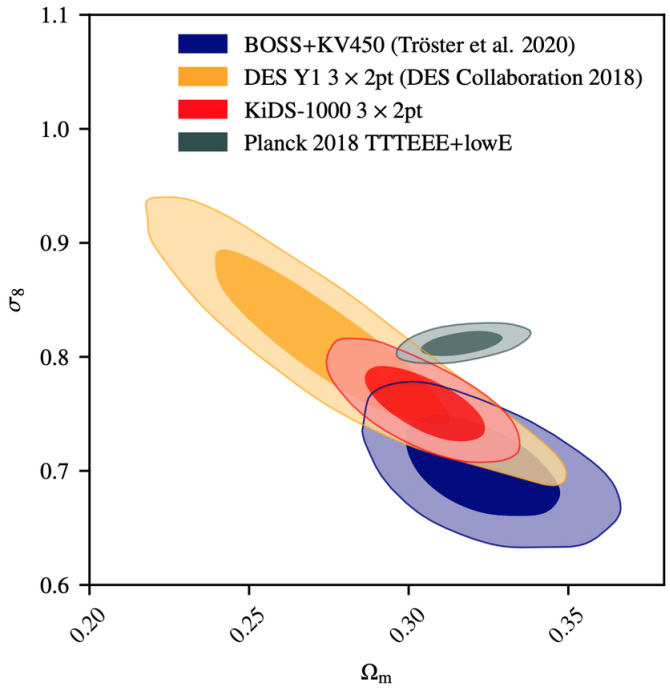

Figure 2: The σ_8 tension visualised, specifically between CMB data (Planck collaboration et al. 2018) and various different large-scale structure surveys: Galaxy clustering from the Baryon Oscillation Spectroscopic Survey (BOSS) team (Tröster et al. 2020), weak gravitational lensing analysis from galaxies imaging (Heymans et al. 2021) and a combination of both survey types seen in the Dark Energy Survey (DES) year one results (Abbott et al. 2018). Image credit: Di Valentino et al. (2021a)

3. The Equations, Properties and Amount of Decaying Dark Matter

We need to mathematically describe DDM in our universe. We do this by first splitting our density of dark matter into two components

$$\rho_{DM}(t) = \rho_{DDM}(t) + \rho_{CDM}(t) \,, \tag{1}$$

where ρ_{DDM} denotes the decaying fraction of the dark matter, whilst $\rho_{CDM}(t)$ denotes our standard, non-decaying cold dark matter. Both are a function of cosmic time. We can relate the overall dark matter density to the decaying and cold densities via the fraction parameter ϵ as

$$\rho_{DDM}(t) = \epsilon\rho_{DM}(t) \qquad \rho_{CDM}(t) = (1-\epsilon)\rho_{DM}(t) \,, \tag{2}$$

and parameterise decays by an exponential with characteristic decay rate parameter Γ ($=1/\tau$, where τ is average the particle lifetime) via

$$\rho_{DDM}(a) = \rho_{DDM_0} a(t)^{-3} \exp(-\Gamma t) \,, \tag{3}$$

where $a(t)$ is the scale factor assuming an FRW universe, with $a_0 = 1$, ρ_{DDM_0} the present-day density of the decaying fraction of dark matter and t cosmic time. Assuming a spatially flat universe, in agreement with recent evidence (Efstathiou and Gratton 2020), we can then fix our Hubble parameter and derive the system of cosmological equations (see Appendix A for explicit derivation details)

$$\boxed{\frac{d\rho_B}{dt} + 3\rho_B\frac{\dot{a}}{a} = 0} \,, \tag{4}$$

$$\boxed{\frac{d\rho_{DM}}{dt} + 3\rho_{DM}\frac{\dot{a}}{a} = -\epsilon\Gamma\rho_{DM}} \,, \tag{5}$$

$$\boxed{\frac{d\rho_R}{dt} + 4\rho_R\frac{\dot{a}}{a} = \epsilon\Gamma\rho_{DM}} \,, \tag{6}$$

$$\boxed{H^2 = \left(\frac{\dot{a}}{a}\right)^2 = \frac{8\pi G}{3}\left(\rho_R + \rho_{DM} + \rho_B + \rho_\Lambda\right)} \,, \tag{7}$$

where we have each quantity as $\rho_B(t)$ = baryon density, $\rho_{DM}(t)$ = dark matter density and $\rho_R(t)$ = radiation density, all as functions of cosmic time. The parameter ρ_Λ, denotes the dark energy density, and is constant in time. We note the form of these Equations, and how the decays are acting as source terms in Equations 5 and 6. This term is positive for radiation evolution in Equation 6, thus increasing radiation density with time, whilst negative for dark matter evolution in Equation 5, decreasing its overall density with time.

3.1 - The Properties of our Decay Products

It is important at this stage to clarify the nature of our decay products. We are considering pure radiation decays of the form

$$\psi \rightarrow \phi + \phi \,,$$

where ψ is a massive parent particle, and ϕ is a massless daughter particle. Crucially, ϕ is a form of dark radiation, not radiation in the form photons. Such a dark matter decay to a form of dark radiation is well-motivated theoretically (Ackerman et al. 2009). We don't expect photons to be produced, or else dark matter

would light up the universe through these decays. In the same way that photons mediate electromagnetic interactions between baryonic matter, dark radiation mediates interactions between dark matter particles. As such, the decay products in a DDM universe are not the same as the radiation sector of the ΛCDM model which consists of photons from the CMB and other various sources and neutrinos (Bond, Efstathiou, and Silk 1980). They have the same effective equation of state ($w = 1/3$), but dark radiation does not contribute to structure formation, only the expansion of the universe. This will be of importance in Section 6, but is mentioned here for completeness. The above boxed equations (equations 4 - 7), can then, with appropriate initial conditions, be evolved to give the behavior of $H(z)$. The initial conditions of our system used in subsequent analysis are described below.

3.2 - Initial Conditions Set on Decaying Dark Matter

We now examine DDM by evolving our system of equations from a redshift of $z = 10$. Doing so, we construct a universe in which no decay of dark matter has occurred for $z > 10$. This is appropriate as we are considering late-time decays, and at $z = 10$ the age of the universe is a small fraction of the Hubble time.

We fix the initial time by using the analytical result for the age of a matter dominated universe. This is valid at redshift $z > 2$ as we approximate the high redshift universe after matter-radiation equality as matter dominated (Weinberg 2008). The explicit form of this equation is given in Appendix A.

For the density of each component, we gain their value at $z = 10$ by assuming ΛCDM fiducial values at $z = 0$, and by the matter-redshift scaling (discussed in Section 2.1), extrapolate these back to $z = 10$. The resulting initial conditions we use in all subsequent analysis is given in Table 1 below.

Parameter	Value at $z = 0$	Value at $z = 10$
ρ_B	4.185×10^{-28}	5.570×10^{-25}
ρ_{DM}	2.284×10^{-27}	2.992×10^{-24}
ρ_Λ	5.870×10^{-27}	5.870×10^{-27}
ρ_R	0	0
t	–	5.728×10^{8}
$a(t)$	1	1/11

Table 1: Initial conditions of Planck used in all subsequent numerical work to evolve our universe from $z = 10$. We note the units of densities to be kgm^{-3} and time t to be measured in years. Scale factor $a(t)$ is dimensionless. The densities at $z = 0$ are listed here to show how they are integrated back to $z = 10$ and are not the final results when DDM is applied. The negligible radiation density in the universe at present day (Planck collaboration et al. 2018) is set to 0 here for convenience. This does not affect our conclusions, as the universe is still fully matter-dominated at $z = 10$.

Our system is then fully defined, and we can numerically evolve the equations from early time ΛCDM conditions under DDM to examine its late-time effects. This is done in Section 4.1.

4. What To Expect in the Decaying Dark Matter Scenario

Before doing a more complex analysis and placing constraints on DDM, we can examine its effect using a simpler analysis. This will help to give us a more quantitative understanding of its effects beyond the qualitative arguments of Section 2.1. Also, it will help us to place in context the results of the more complex analysis in Section 5, and assure us of both the qualitative and quantitative nature of these results. We start by reconstructing the expansion history for various values of Γ in our DDM universe.

4.1 - The Expansion History of Various Universes

Using the initial conditions discussed in Section 3.2 and given in Table 1 we can reconstruct the expansion history (the Hubble parameter as a function of redshift) of the universe for varying values of the decay constant Γ. We apply a fourth order Runge-Kutta (RK4) numerical solver to our system of Equations 4, 5, 6 and 7 with steps made in cosmic time. The evolution of the Hubble parameter from $z = 10$ is given in Figure 3 below.

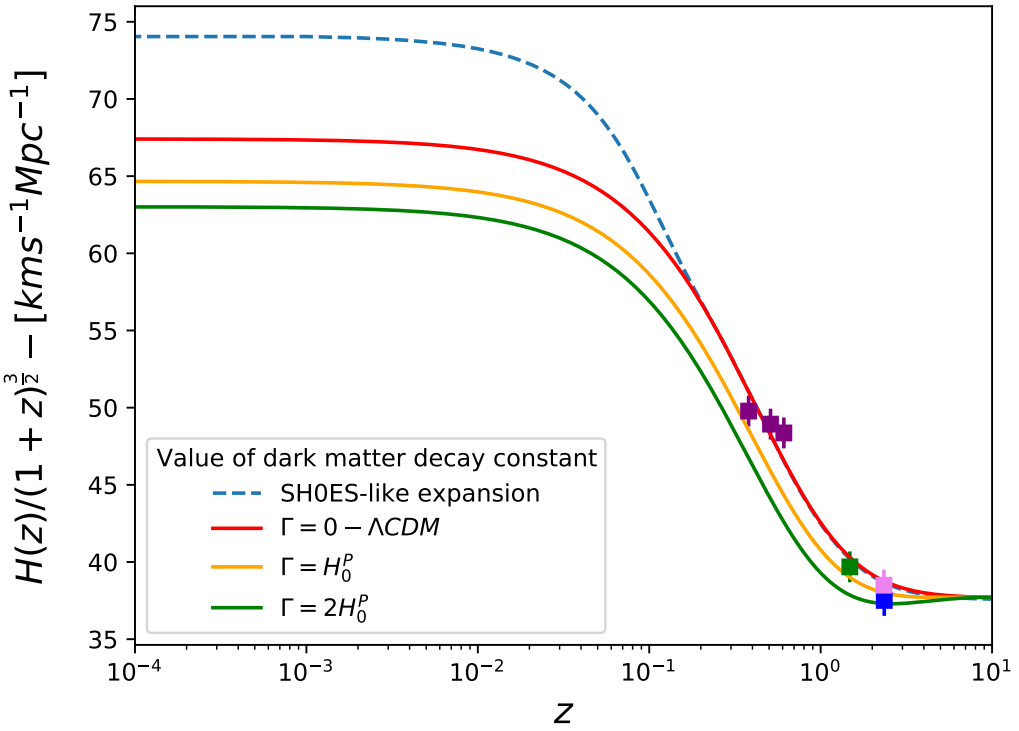

Figure 3: The evolution of the Hubble parameter from redshift $z = 10$, with different values of the decay constant Γ, with $\epsilon = 1$. We note the decreasing value of the Hubble parameter at ultra-low redshift for larger decay constant. The dashed line shows the kind of expansion that would be required to get the SH0ES value of the Hubble parameter at z=0 (following the model-independent parameterisation approach of Lemos et al. (2018)). Clearly they are not reconciled by decays. The three purple points show $H(z)$ in different redshift bins from the Baryon Acoustic Spectroscopic Survey (Alam et al. 2017). The green point at $z = 1.48$ shows $H(z)$ from correlation of quasars (Zhao et al. 2022). The pink point at $z = 2.34$ shows $H(z)$ measured from correlations of Lyman$-\alpha$ absorbers (Sainte Agathe et al. 2019) whilst the blue point at $z = 2.35$ shows $H(z)$ from cross-correlation of Lyman$-\alpha$ absorbers and quasars (Blomqvist et al. 2019) following Efstathiou (2021). The values of Γ used here are multiples of the Planck value of the Hubble parameter, H_0^P, as discussed and defined in Section 2.1.

We note the normalisation of $(1+z)^{1.5}$ on the y-axis giving the apparent 'kinks' at $z \approx 1.5$ for larger values of the decay constant Γ. We immediately see that the SH0ES value of the Hubble parameter at redshift $z = 0$ is not recovered, and DDM serves only to decrease the value of H_0 (as we expected from redshift-diluting arguments in Section 2.1). The curves match at $z = 10$ as we'd expect, as all curves share the same initial conditions. We note the coloured points from BOSS, Lyman-α absorber and quasar data. These data are not used to constrain these curves. They will be used in Section 5 to allow us to constrain our value of Γ via MCMC methods, where these measurements will help define likelihoods within our parameter space via an inverse distance ladder approach, following the methods of Efstathiou (2021).

4.2 - Magnitude - Redshift Relations and Decaying Dark Matter

We can also explore the behaviour of our DDM in matching the expected apparent magnitude redshift relations from SNIa of the Pantheon Supernovae Sample (Scolnic et al. 2018).

As done previously in Section 2.1, we can adopt a spatially flat geometry (Efstathiou and Gratton 2020). The Hubble parameter then fixes the redshift-dependent luminosity distance $D_L(z)$ to an astrophysical source in an FRW universe by

$$D_L(z) = c(1+z)\int_0^z \frac{dz'}{H(z')}\,, \tag{8}$$

where c is the speed of light and z is redshift. Standard candles and standard rulers can then be used to constrain the history of $H(z)$ independent of any dynamics (Heavens, Jimenez, and Verde 2014; Bernal, Verde, and Riess 2016; Lemos et al. 2018). We have an apparent magnitude formula given by

$$m_B(z) = M_B + 25 + 5\log_{10} D_L(z)\,, \tag{9}$$

where $D_L(z)$ is the luminosity distance given in mega-parsecs, M_B is the peak absolute magnitude of the source and $m_B(z)$ is the redshift dependent peak apparent magnitude of the source. The role of the Hubble parameter in Equation 8 then allows us to link the luminosity distance to the expansion history of the universe. We can then investigate how Γ affects the fit of theoretical apparent magnitude curves against actual data, by using the formula for D_L in Equation 9 and the Pantheon team's results respectively. In doing this, we proceed in the same way as the method used for Figure 3, but now also numerically integrating following the formulae of Equations 8 and 9.

It is also important to understand the supernovae sample we are using to compare our theory to observables. The pantheon supernovae survey (Scolnic et al. 2018) reports results on the peak apparent magnitudes of 1048 SNIa, measuring their magnitudes in both heliocentric and CMB rest frames. The CMB rest frame magnitudes are used in our own analysis and plotted in Figure 4. Obtaining these magnitudes is a complex process including analysis of light curves and photometric calibrations (more details in Freedman et al. (2020)). The resulting data is then used primarily in the SH0ES team work for fitting these SNIa to the Hubble flow to determine a value of H_0^S, but can also be used to determine cosmological parameters itself. In the process of completing this project, the Pantheon team released their full, extended analysis of 1701 light curves from SNIa (Scolnic et al. 2021). This included more SNIa data, and allowed for Riess et al. (2021) to further improve upon their own work. Its results do not affect our own conclusions. The result of our own analysis is seen in Figure 4 overleaf.

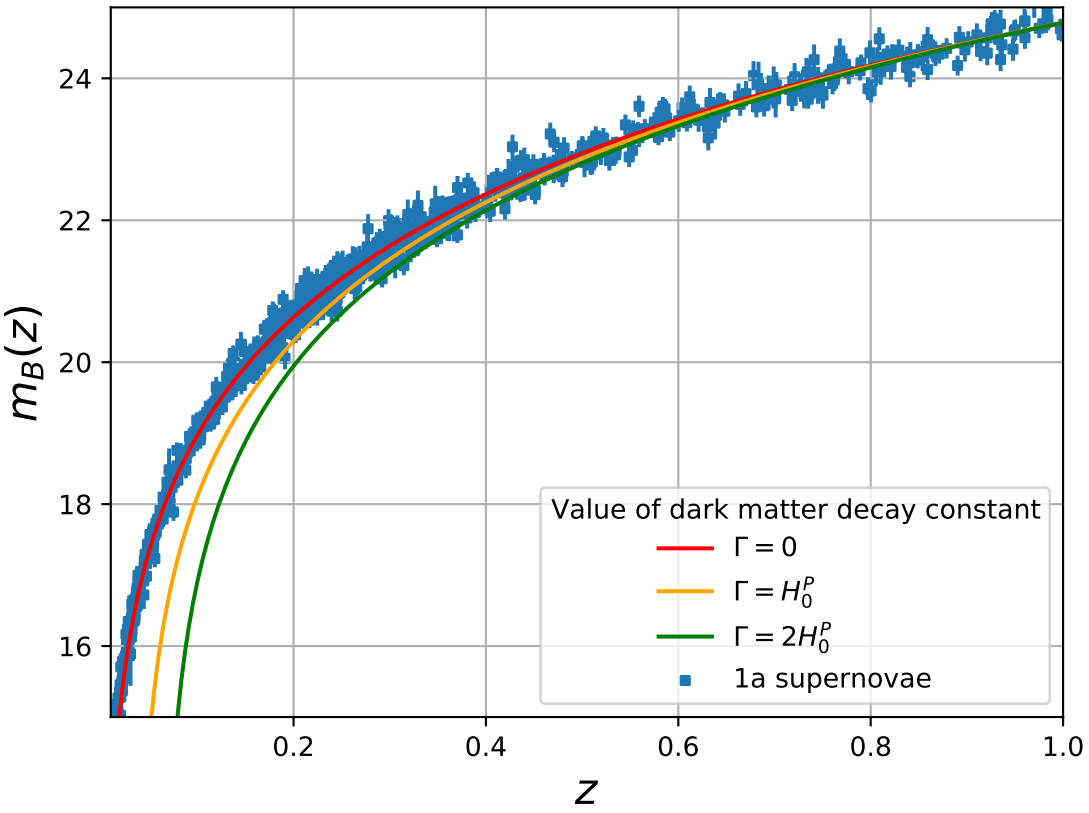

Figure 4: Peak apparent magnitude of numerous SNIa from the pantheon supernova sample (Scolnic et al. 2018) with fits from theory for varying expansion histories. A value of $M_B = -19.4$mag is used here. 1σ Error bars are plotted with each supernova. We note the deviation of the non-ΛCDM cosmologies from the observed SNIa magnitudes.

From Figure 4, we can see that this low redshift supernovae data will place very tight constraints on the value of Γ, and so we can anticipate a value of $\Gamma \ll H_0^P$ to be consistent with this dataset to an acceptable degree of error. The data does not *want* decays to occur.

It is interesting to note that this fit is made with $M_B = -19.4$mag, which is in conflict with the fit from SH0ES, which matches the Pantheon sample to the Hubble flow with $M_B \approx -19.2$mag. In contrast, ΛCDM priors fit the pantheon supernovae sample with $M_B = -19.4$mag. This again feeds into the H_0 tension, which from a SH0ES perspective can be thought of as a SNIa peak magnitude tension of ≈ 0.2mag (Vagnozzi 2021). The peak absolute magnitude of $M_B = -19.4$mag used here is to give the fit is consistent with the value obtained from using ΛCDM priors, which we ourselves have used, mirroring the same constraint placed on M_B by Efstathiou (2021).

Crucially, as we move forward to more complex constraining methods, we can already see that the observational data we are using in Figures 3 and 4, SNIa and various baryon acoustic oscillation (BAO), Lyα and quasar data, do not want dark matter to decay. The deviations from observed supernovae are too large for an acceptable degree of error, even for $\Gamma = H_0^P$. We expect a very small value of Γ to be produced when we constrain against this data set. This is confirmed in the following Section.

5. The H_0 Tension Investigated in a Decaying Dark Matter Universe

We now know what we should expect in a DDM universe: A value of $\Gamma << H_0^P$ (for $\epsilon = 1$), such that $H(z)$ is consistent with SNIa magnitude data, and a universe hardly effected by decays. But what actual values (and confidence in those values), can we associate with Γ? And how do the values of other parameters behave in a DDM universe? It is the goal of this Section to perform a deeper analysis, using an inverse distance ladder and an MCMC analysis (described in more detail below) of DDM, aiming to answer these questions.

5.1 - $\epsilon = 1$

The inverse distance ladder method works as follows: If we assume a flat universe (as done in Section 4.2), then luminosity (and angular diameter) distances (Equation 8) are fixed exactly by $H(z)$. We then assume a value of the sound horizon, which then fixes $H(z)$ from BAO data (as plotted in Figure 3). SNIa data then constrains value of $H(Z)$ to low redshift. We then have a model independent method of constraining $H(z)$, which we can constrain relative to our own model using the MCMC method (more details in Lemos et al. 2018).

The MCMC method is a Bayesian statistical analysis tool that assesses the confidence one can have in a parameter (or collection of parameters) having a specific value. The MCMC method permutes through a number of different parameter value configurations, aiming to minimise the likelihood function given in Equation 11. The result (in our case) is an 11 dimensional parameter landscape having been shaped to maximise likelihood defined and shaped by our astrophysical datasets. We can then image this in 2D planes to get confidence contour plots for our parameters.

The case of the decay fraction parameter $\epsilon = 1$ corresponds to all of the dark matter in the universe having the possibility of decaying. Restricting ourselves to this case for the time being, we can construct a cosmological parameter space. We can then run an MCMC analysis and investigate the confidence of our parameters lying in specific ranges. The main aim with this analysis is to constrain the decay constant Γ with H_0 to assess how the value of H_0 behaves with decays when constrained against BAO and SNIa data. The details used to achieve this are outlined below.

We must place prior ranges and distribution on parameters we wish to analyse. The priors used in our analysis are all uniform (they have the same likelihood value for all parameters in their prior range), except for the sound horizon r_d[3], which has a Gaussian prior. We use a Planck-based Gaussian prior (Planck collaboration et al. 2018), as in the resulting analysis the sound horizon directly affects BAO data (as discussed above). As such, we set $r_d^{\Lambda CDM} = 147.27$Mpc, and the resulting χ^2

$$\chi^2_{r_d} = \frac{(r_d - 147.27)^2}{2\sigma^2_{r_d}} \, . \tag{10}$$

Where $\sigma^2_{r_d}$ has the Planck value of 0.31 Mpc^2 (Planck collaboration et al. 2018). We use Gaussian priors on all other data used in constraing our likelihood, again following the inverse distance ladder of Efstathiou (2021), and construct a likelihood function L that follows

$$-2\ln \mathrm{L} = \sum \chi^2 = \chi^2_{r_d} + \chi^2_{SN} + \chi^2_{BOSS} + \chi^2_{6DF} + + \chi^2_{QSO} + \chi^2_{Lya_1} + \chi^2_{Lya_2} \, . \tag{11}$$

Here each term in the above corresponds to the associated χ^2 value of the sound horizon (Planck collaboration et al. 2018), SNIa peak magnitude (Scolnic et al. 2018), the BOSS team's values of $H(z)$ (Alam et al. 2017), results from quasar analysis (Zhao et al. 2022), cross-correlation analysis of quasars and lyman-α absorber (Blomqvist et al. 2019) and Lyman-α cross-correlations (Sainte Agathe et al. 2019).

[3]The sound horizon is the distance travelled in the early universe by baryon overdensities propagating as acoustic sound waves before baryons decoupled from photons. This radius is the same for all over densities.

We use the MULTINEST algorithm (Feroz and Hobson 2008) for our MCMC analysis to explore the parameter space. We aim to minimise (by the minus sign of Equation 11) the "log-likelihood" in the parameter space we offer. The parameters we use and their fits, along with their prior ranges, are listed in Table 1 with $\pm 1\sigma$ errors. Derived parameters, indicated by lack of prior, are also given. In Table 2 below, and all that follows, the units of H_0, H_0^S and Γ are $\mathrm{kms}^{-1}\mathrm{Mpc}^{-1}$. The unit of r_d, the sound horizon, is Mpc, and the unit of M_B, the SNIa peak absolute magnitude is magnitude.

Parameter	Fit	Prior Range
Ω_B^F	$0.056^{+0.0069}_{-0.012}$	$0.04 - 0.05$
Ω_{DM}^F	$0.2629^{+0.0079}_{-0.017}$	$0.25 - 0.27$
Γ	$0.056^{+0.17}_{-0.60}$	$0 - 50$
M_B	$-19.42^{+0.025}_{-0.030}$	$-19.5 - -19.0$
r_d	$147.39^{+0.76}_{-0.77}$	$146 - 149$
Ω_B	$0.0537^{+0.0073}_{-0.012}$	–
Ω_{DM}	$0.245^{+0.025}_{-0.045}$	–
Ω_M	$0.299^{+0.023}_{-0.042}$	–
Ω_R	$0.0103^{+0.029}_{-0.011}$	–
H_0	$67.47^{+0.57}_{-0.79}$	–
H_0^S	$67.37^{+0.74}_{-0.90}$	–

Table 2: Parameter fits and prior ranges with associated $\pm 1\sigma$ errors. The density fraction parameters Ω are all measured at $z = 0$. Subscripts B, DM, M and R refer to baryons, dark matter, matter and radiation components respectively. The superscript marker F refers to the fiducial values of the density parameteres used, which are then scaled back to $z = 10$ (as in Section 3) and hence evolved to present day by applying the MCMC method. Note that discussion of the parameter H_0^S is not important to our DDM investigation and so is discussed in Appendix B.

In performing the MCMC analysis, we use the method of Section 4.2, reconstructing the expansion history for a varying set of initial conditions set by each parameter configuration. Each resulting expansion history

then has an associated likelihood by comparisons with datasets being used. Prior ranges on fiducial values of density fractions Ω are taken to include accepted ΛCDM values, with the negligible radiation density set to 0, consistent with CMB data (Planck collaboration et al. 2018).

Crucially, we are constraining our value of Γ in this analysis from a large prior range, such that after a large number of iterations the MCMC algorithm has converged to maximise likelihood to a sufficient degree of accuracy. The resulting two-dimensional contour plots of a number of parameters are given in Figures 5, 6 and 7 below.

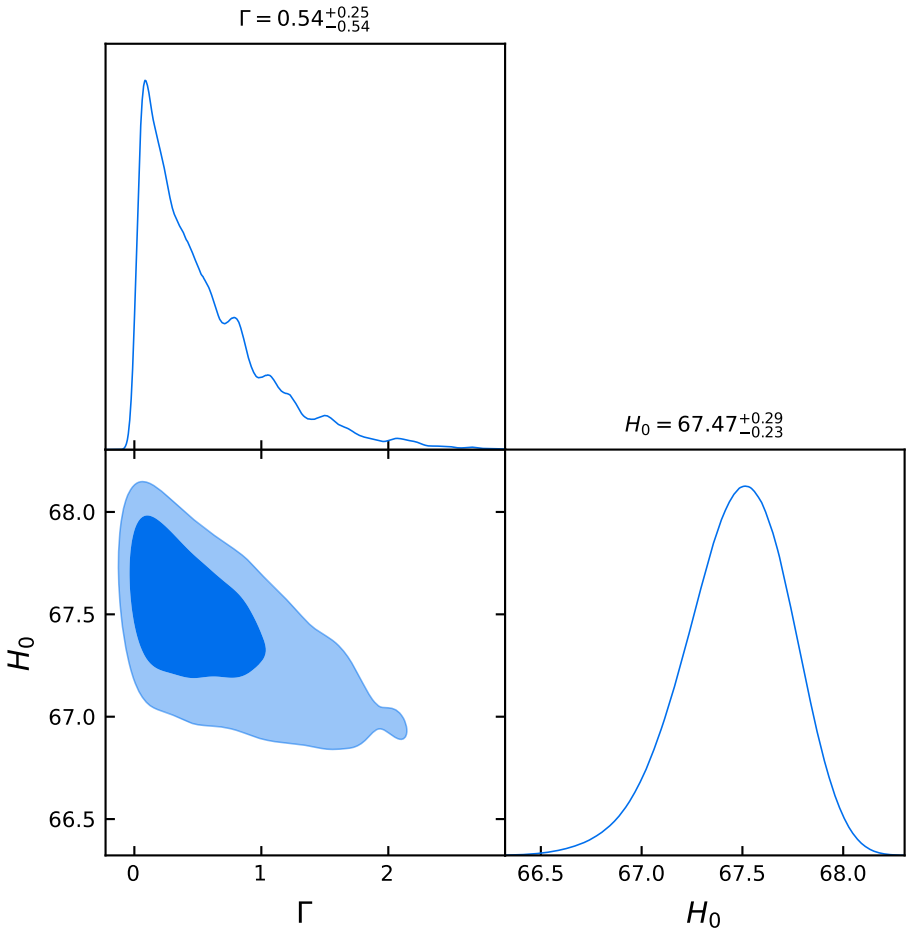

Figure 5: We see this confidence plot detail exactly what we have previously expected. A larger value of our decay constant Γ gives a lower value of H_0, seen by the 'sheared' shape of this plot. We see that for $\Gamma = 0$, the Planck value, $H_0^P = 67.4 \pm 0.5$ kms^{-1}Mpc^{-1}, is recovered. The higher SH0ES value of H_0 is not recovered. This plot, and all subsequent plots of this nature are made with the `GETDIST` python package (Lewis 2019), where darker blue regions correspond to 1σ condifence intervals, and lighter blue regions are 2σ confidence intervals.

In this plot here we have achieved the minimum aim of the project. We have constrained decaying dark matter to a decay rate constant of $\Gamma = 0.54^{+0.25}_{-0.54}$ kms^{-1}Mpc^{-1}, an average lifetime of $\tau \approx 528$ billion years. A lifetime much longer than the age of our universe. This is consistent with our argument against DDM offering a solution to the H_0 tension in the discussions of Section 2.1 and Figure 3. The data we have used from the late time universe clearly do not want decays, and in any case DDM in our universe serves to only worsen the Hubble tension. We can now also examine the behaviour of our fractional density parameters Ω with DDM. This is seen overleaf.

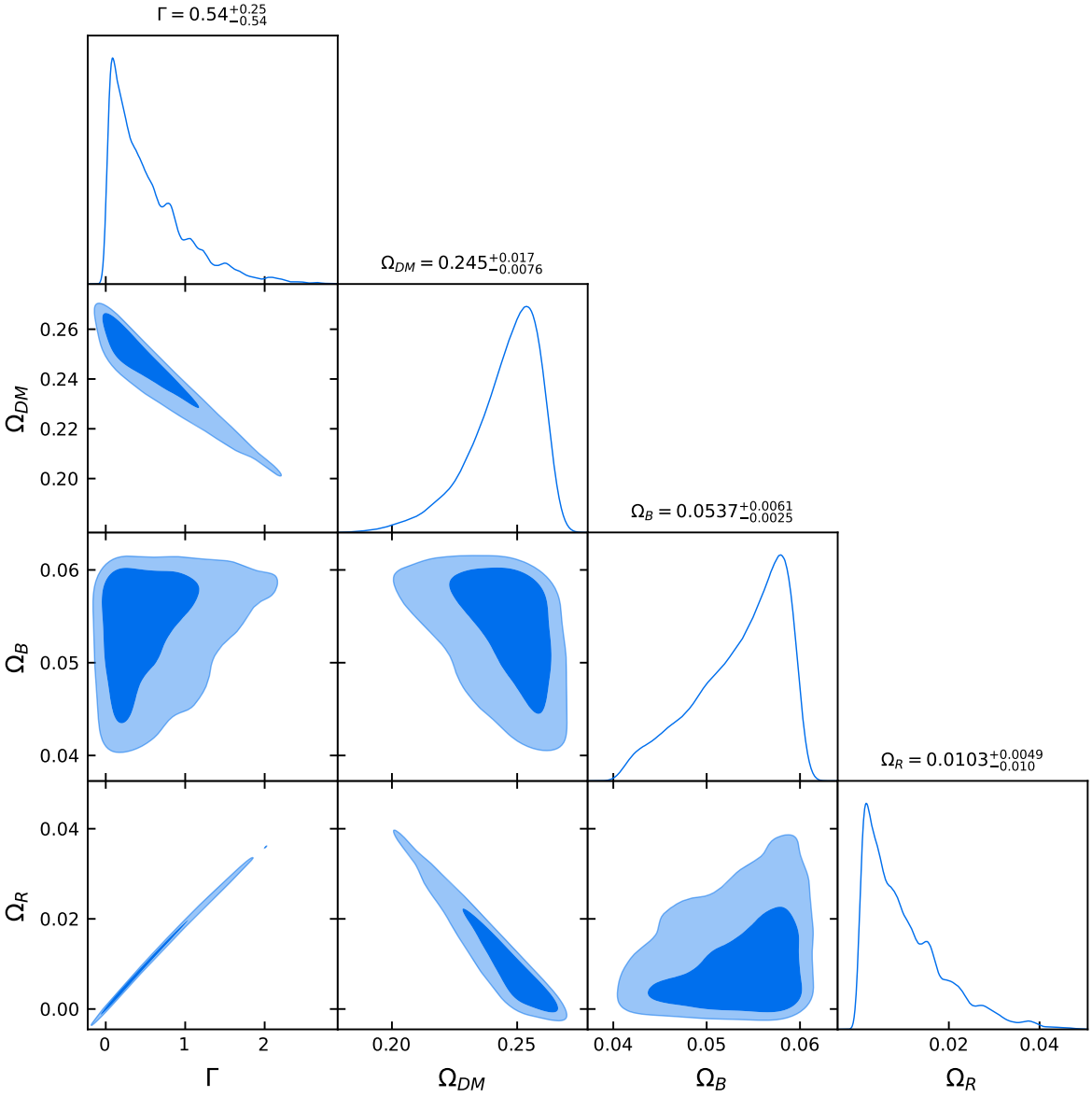

Figure 6: A triangle plot of the radiation, dark matter and baryon density fraction parameters in the context of our decays. We see what we expect qualitatively: Ω_{DM} decreases with increasing Γ, and so decays away to (dark) radiation, whose density Ω_R is seen to then increase with Γ. Ω_B is within its Planck value. Our decays are hence behaving as we'd expect.

All parameters seen in the ΛCDM models have values are constrained to within 1σ of their Planck values. This is consistent with a DDM universe that barely decays. We can the also examine the behaviour of Γ with constrains on the SNIa peak magnitude and sound horizon.

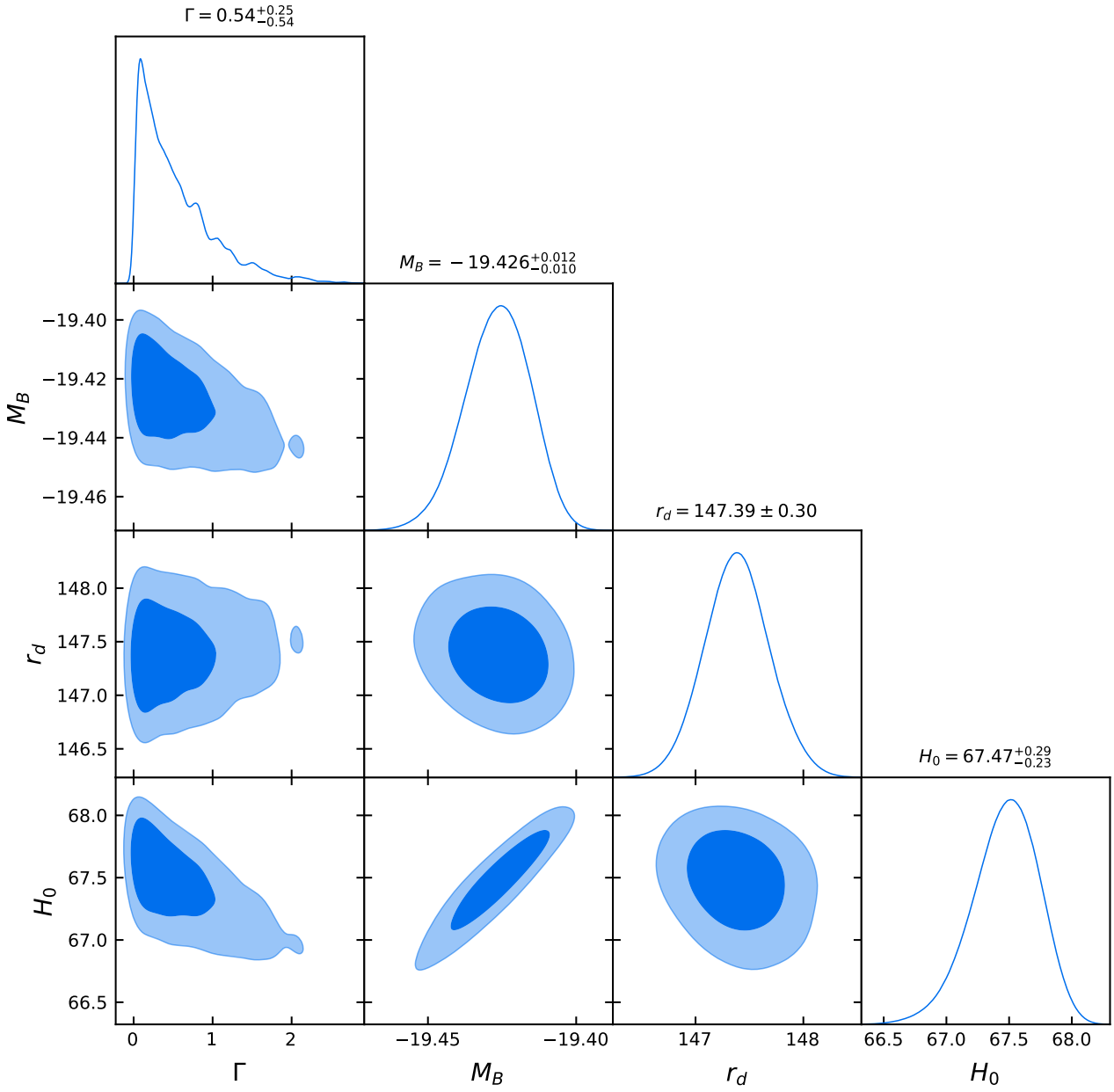

Figure 7: A triangle plot showing constraints of peak SNIa magnitude and the sound horizon value. Again we note our value of M_B to be constrained to a value consistent with ΛCDM values. The sound horizon itself is constrained neatly within its Planck value.

From these plots, we can see that the value of the sound horizon is not affected by the presence of a DDM. This was to be expected: DDM does not alter the sound horizon, and so the graph of Γ vs r_d exhibits no perceptible slope. A similar situation is seen for M_B. Both the sound horizon and peak 1a magnitude values are generally insensitive to our dark matter decay constant. The behaviour of H_0 with M_B and r_d is consistent with a ΛCDM cosmology (Efstathiou 2021; Planck collaboration et al. 2018).

5.2 - $\epsilon \neq 1$

The case of $\epsilon \neq 1$ corresponds to only a fraction the dark matter in the universe having the possibility of decaying. We can explore this possibility by introducing ϵ as a varied parameter in our MCMC likelihoods over its full range: $\epsilon \in [0, 1]$, set as a uniform prior. On re-running our analysis, incorporating ϵ, the most interesting plot we gain is the one of our decay fraction ϵ with decay parameter Γ. This is seen in Figure 8 below.

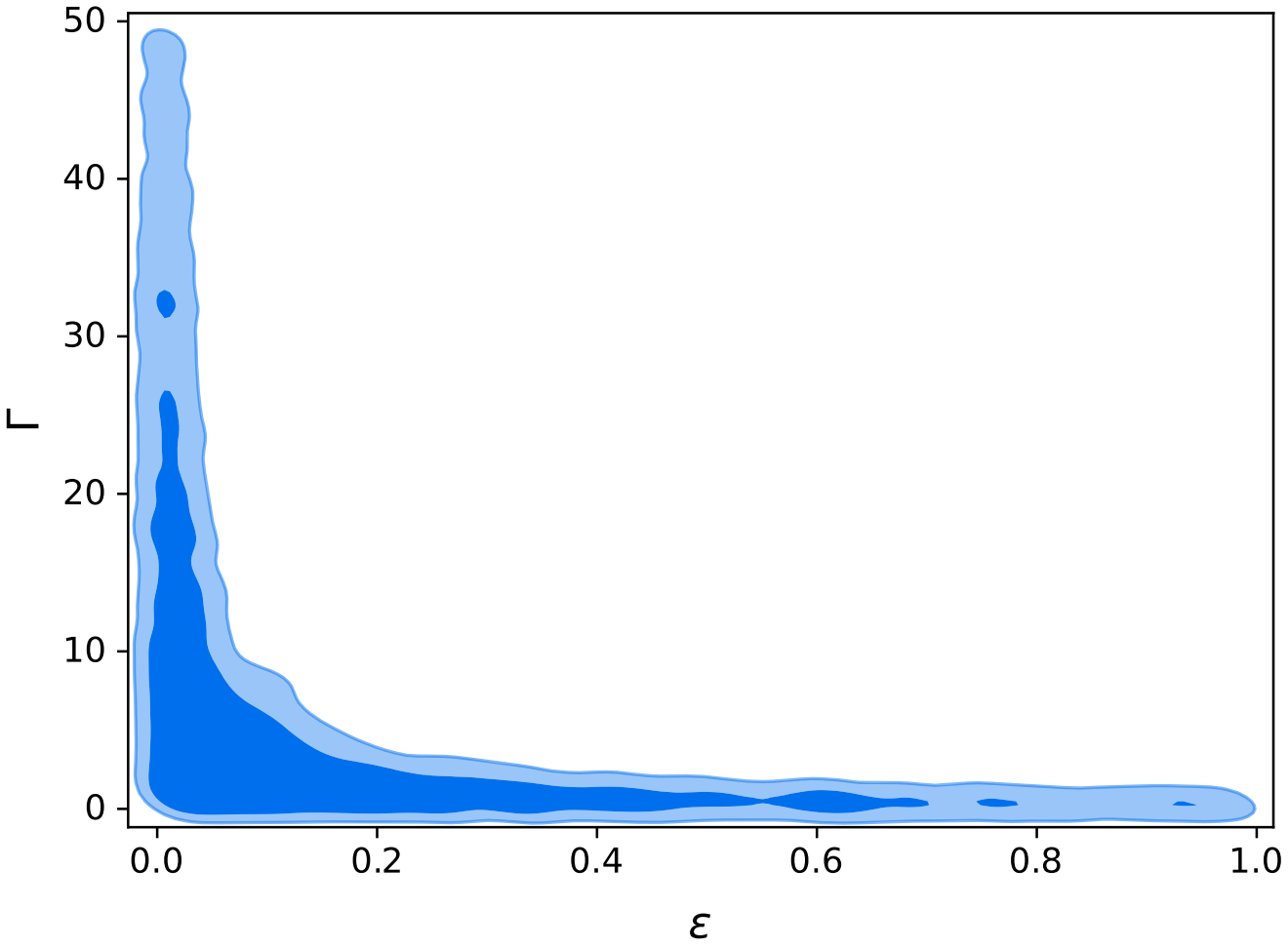

Figure 8: We see that for low values of ϵ permit large values of Γ. A small decaying fraction will mean that the value of H_0 is not affected (as such a small component of dark matter decays away), but the dark matter that is subjected to decays will do so on a timescale much shorter than the expansion timescale. This has interesting consequences for structure formation.

The nature of the constraints used in our MCMC that define our likelihoods naturally allow for a universe in which, if only a small fraction dark matter decays, it may do so on timescales comparable to the Hubble time, as this small fraction does not skew the rest of the cosmological parameters outside ranges allowed by our inverse distance ladder. So, a universe may permit DDM with an average lifetime comparable to the Hubble time, if and only if a small fraction of the dark matter in the universe is subject to decays. In essence, late time universe data is consistent with a ΛCDM model, but if only a very small fraction of the energy budget deviates from ΛCDM, this may be permitted. With timescales of decays on a Hubble time in this fractional case, this may give some effect on structure formation up to the present epoch. This motivates our investigation into structure formation, that we now turn our attention to.

6. Structure Formation and the σ_8 and S_8 Tensions with Decaying Dark Matter

Our analysis of the validity of DDM offering a solution to the Hubble tension is complete. We have seen that it offers no such solution, and this form of late-time deviations from ΛCDM cannot help alleviate the tension. However, an analysis of structure formation with DDM may tell a different story for the σ_8 and S_8 tensions. We proceed with our analysis, turning our attention to the evolution of matter over-densities (rather than the average matter density), setting $\epsilon = 1$ throughout to maximise the effects of DDM, having demonstrated that $\epsilon \neq 1$ allows for some decays to occur on a Hubble time.

6.1 - The Evolution of the Linear Overdensity Field

The linear overdensity in the matter density field, δ, evolves via the linear growth equation, which is

$$\boxed{\ddot{\delta} + 2H\dot{\delta} - 4\pi G\bar{\rho}_m\delta = 0}\,. \tag{12}$$

We see how our decays will enter this equation and impact growth: Through the evolution of both $H(z)$ and $\bar{\rho}_m$. The equation will permit a linear growth parameter $D(z) \propto \delta(z)$ which we can numerically solve for. Noting the arguments of Section 3.1, we expect our dark radiation decay component not to contribute to structure formation (i.e. will not be present in the $\bar{\rho}_m$ term in Equation 12. Coupling this equation to our other conservation equations with ΛCDM initial conditions at $z = 10$, and solving for $D(z)$, gives our growth of structure with redshift: $D(z)$ with z. For this analysis we set the decay fraction $\epsilon = 1$. This behaviour of $D(z)$ is seen below in Figure 9.

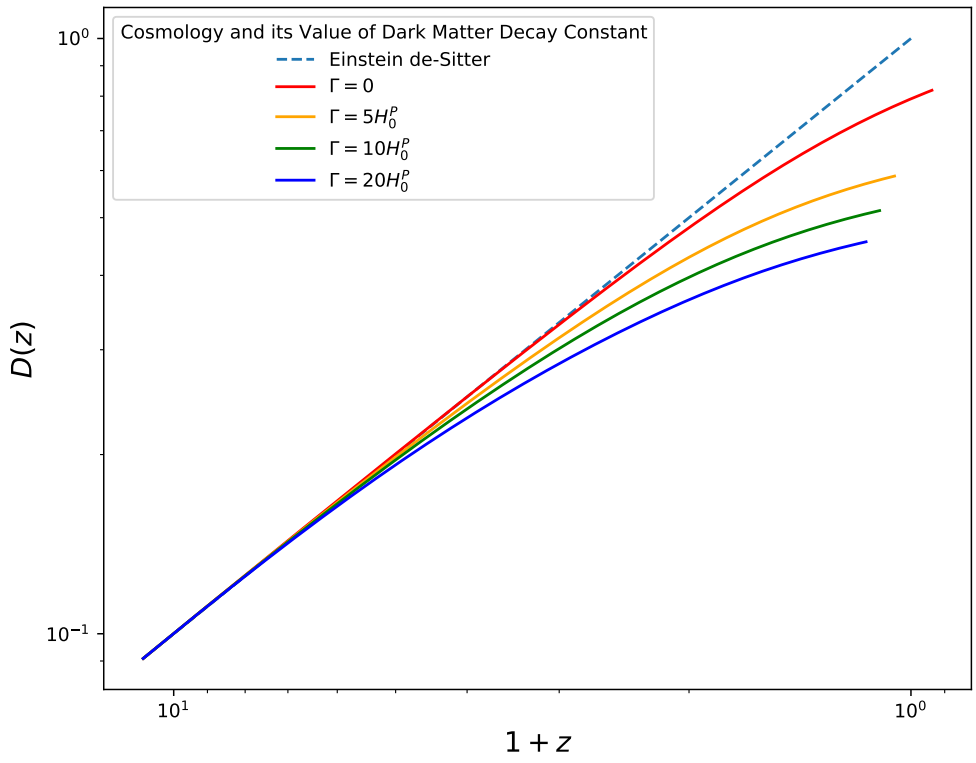

Figure 9: The linear growth rate $D(z)$ is plotted here for a value of ranges of the decay parameter Γ.

From Figure 9, we see that for larger values of Γ the growth rate tends towards an asymptote (becoming near horizontal and constant with redshift). We expect this, as any radiation density will not contribute to the growth of structure as radiation stagnates growth (Meszaros 1974). The growth rate is not full suppressed to a complete asymptote (i.e our growth curves do not become fully horizontal, with $dD(z)/dz \neq 0$ along the whole curve), as our baryons are unaffected by decays and still contribute to structure growth as we'd expect (Weinberg 2008). Even the ΛCDM universe experiences some 'drop-off', as at late times dark energy becomes dominant and this suppresses structure growth as well as radiation, hence the deviation from the Einstein-de Sitter universe.

It is important to note in this analysis that in Equation 12 the term $\bar{\rho}_m$ contains both our dark matter and baryons, as both contribute to structure formation. The act of coupling our equations to those used in Section 4.2 necessarily involves separating Equation 12 into two first-order ODE's that we can then solve numerically. This is discussed more below.

6.2 - Structure Parameters at $z = 0$

We can hence utilise this evolution of our linear perturbations to understand the behaviour of the σ_8 and S_8 parameters. We can relate our derived σ_8 to the ΛCDM value via ratios of our linear growth rate as

$$\sigma_8 = \sigma_8^{\Lambda CDM} \times \frac{D(z=0)}{D_{\Lambda CDM}(z=0)} \, ,$$

where in this analysis we use the Planck value of $\sigma_8^{\Lambda CDM} = 0.8102 \pm 0.0060$, consistent with our previous work in Section 4.2, which used Planck fiducial values. We incorporating both parameters, σ_8 and $D(z)$ into our MCMC analysis with Planck initial conditions again at redshift $z = 10$. We set a small Gaussian prior on σ_8, for the same reasoning we gave for choosing a Gaussian prior on the sound horizon. We note two conditions are needed to incorporate Equation 12 into our previous system of equations, as it is a second order differential equation. These are 'derived' initial conditions, set by fiduciual values of the density parameters and equations. The fits and prior ranges of the newly added parameters from this analysis are given in Table 3 below.

Parameter	Fit	Prior Range
σ_8^F	0.809 ± 0.005	$0.80 - 0.82$
σ_8	$0.8075^{+0.059}_{-0.0048}$	-
S_8	$0.803^{+0.015}_{-0.083}$	-

Table 3: Fits and priors on σ_8 as well as its fiducial value, σ_8^F, and S_8. No priors are on σ_8 or S_8 as they are derived parameters.

What the results of this extended analysis offer us in terms of sourcing a solution to the σ_8/S_8 tensions is hard to visualise without making a direct comparison with Planck and large-scale structure survey data. Such a comparison is made in Figures 10 and 11 for σ_8 and S_8 respectively. The explicit fits for each data set are given in Table 4

	σ_8	S_8
DDM	$0.8075^{+0.059}_{-0.0048}$	$0.803^{+0.015}_{-0.083}$
Planck	0.8096 ± 0.0074	0.828 ± 0.015
Planck + PLens	0.8104 ± 0.0060	0.829 ± 0.012
KiDS - 1000	0.894 ± 0.095	0.766 ± 0.018

Table 4: A comparison of the values and errors we are visualised. It is important to understand what we mean by 'PLens'. This is data from the Planck team having analysed the lensing of their CMB photons as well as their temperature and polarisation (Planck collaboration et al. 2018). It is not a combination of Planck with another large scale structure survey. This data set is used throughout Figures 10, 11 and 12.

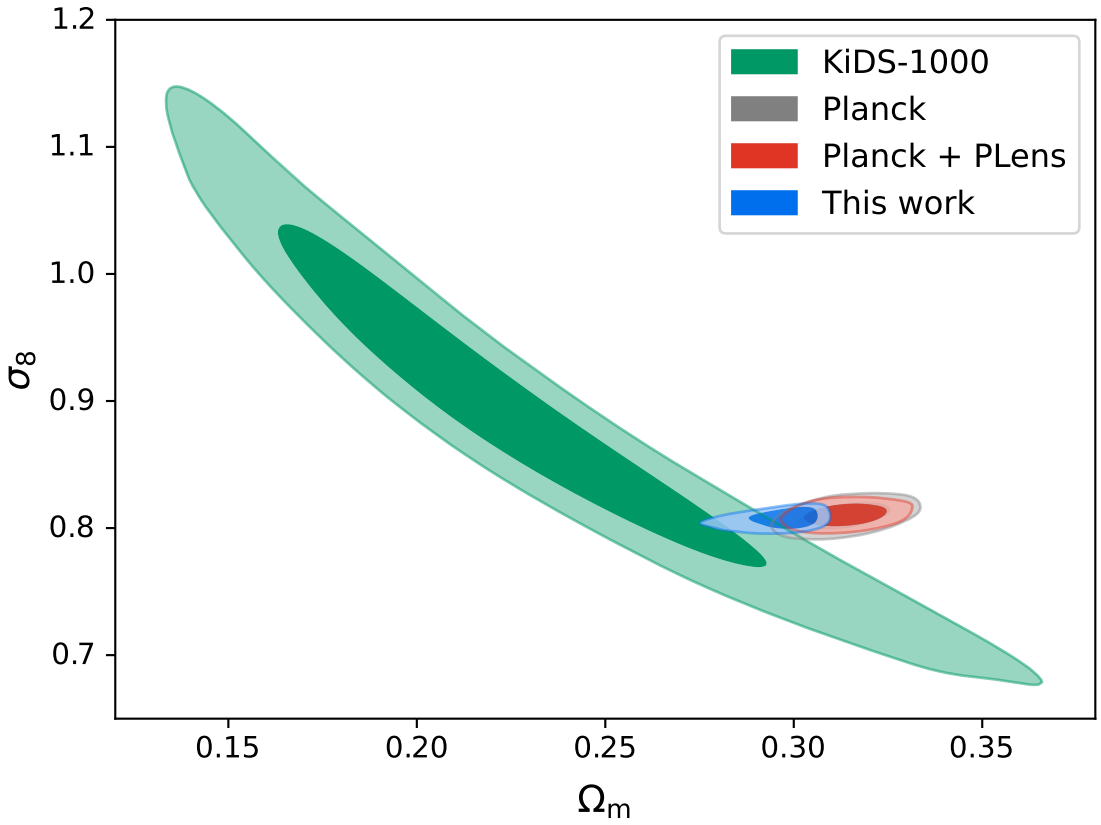

Figure 10: The structure parameter σ_8 with Ω_m under a range of data sets. We see Planck and Planck+Lensing data is not in agreement with weak lensing data by the KiDS team. We then see that our decays in fact reconcile the two to a more acceptable degree of error.

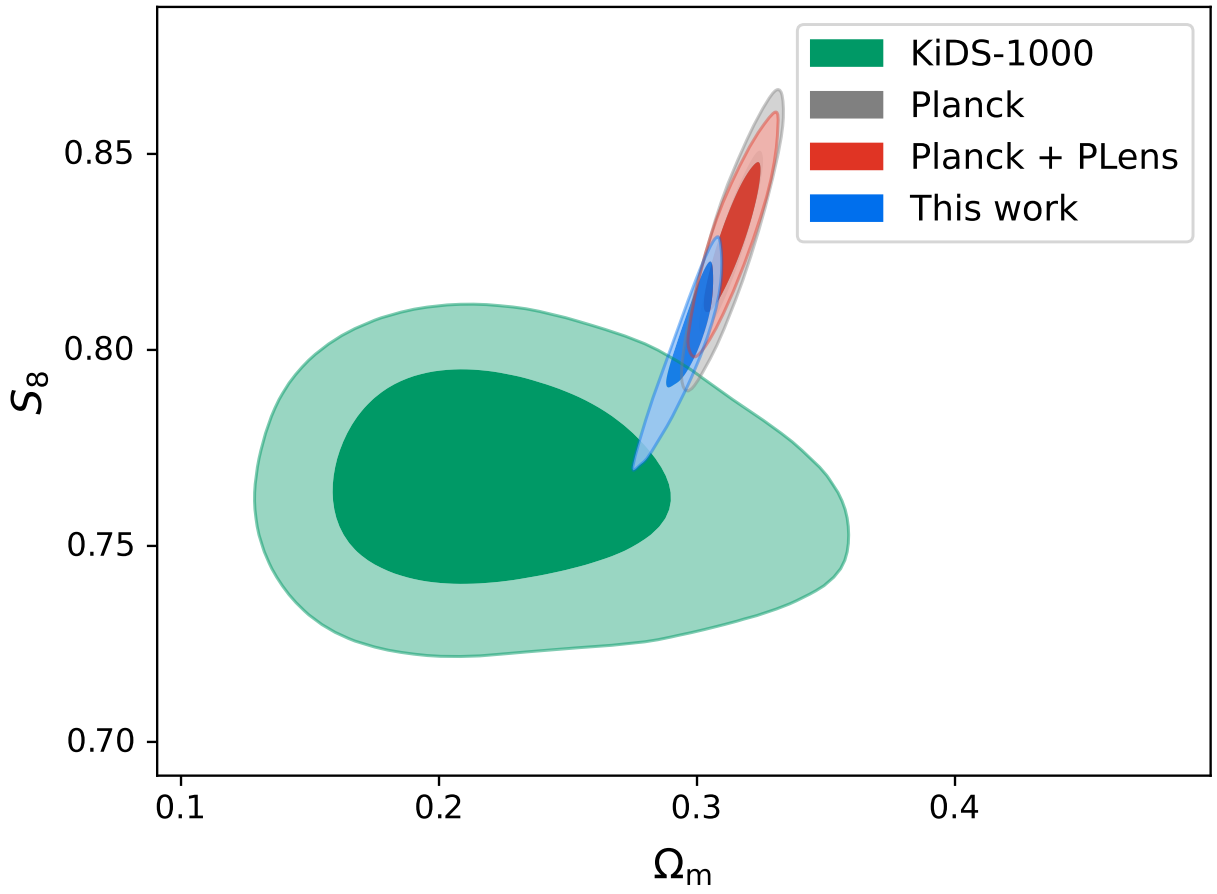

Figure 11: The structure parameter S_8 with Ω_m under a range of data sets. We see Planck and Planck+ Planck Lensing data is discrepant with weak lensing data from the KiDS team. We then see that allowing our decays leads to more overlap with the KiDS results.

For both parameters, we see how decays lead to more overlap between the different datasets of the CMB and galaxy-lensing. It is important to note how throughout this analysis we have only considered $\epsilon = 1$. This scenario gives us the most drastic effect in terms of DDM's effect on structure at $z = 0$, and so is of the most interest to us. Repeating the analysis for $\epsilon \neq 1$ yields results that have less overlap, and of no other real interest.

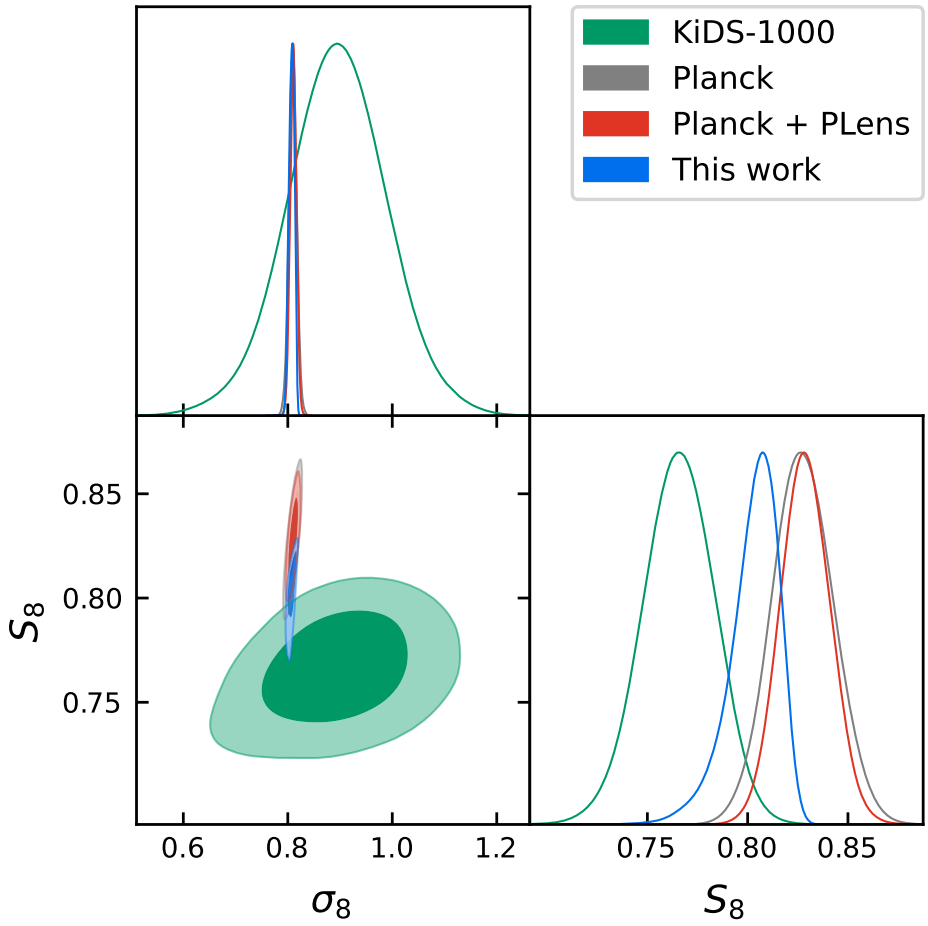

Figure 12: A 1D and 2D plot to further highlight the effect of DDM on the σ_8/S_8 tensions. We can see the results are more explicit for S_8 than for σ_8. The "overlaps" are not as explicit as in Figures 11 and 12, as this overlap is demonstrated mainly in the "tails" (2σ part) of the contour maps.

This analysis shows us that DDM, whilst it offers more overlap between datasets, does not offer a complete solution to the σ_8/S_8 tensions. Instead, the tensions are made slightly more 'palatable', but not by much. The results of Figure 12 highlight to us how in fact the overlaps are not completely satisfactory. In light of these results, it is not possible to conclude that DDM offers a solution to the σ_8/S_8 tensions. This conclusion is not as solid as the conclusions made in Section 5 with regards to the H_0 tension, but the nature of the conclusion remains the same: DDM does not offer a fully satisfactory solution to the σ_8/S_8 tensions.

However, this analysis compares S_8 and σ_8 at $z = 0$. What is the effect on structure at $z > 0$, beyond the information offered by Figure 9? This is addressed in the next subsection.

6.3 - Structure Parameters at $z \neq 0$

The S_8 parameter is defined at $z = 0$. However, we can extend this definition to encompass a range of redshifts. If σ_8 is the variance in the overdensity field, then we can measure this at different redshifts. We then have the definition for a redshift dependent S_8 given as

$$S_8(z) = \sigma_8(z)\sqrt{\frac{\Omega_m}{0.3}}\,, \tag{13}$$

where we use a value of Ω_m set at present day. We can then examine the redshift dependence of our S_8 parameter. We do this by running our MCMC algorithm, sampling the value of S_8 at eight different redshift nodes as in García-García et al. (2021). Here we use $z = \{0,\ 0.06,\ 0.12,\ 0.24,\ 0.35,\ 0.53,\ 0.83,\ 1.5\}$. We can then use a quartic spline interpolation to connect these nodes to produce a confidence plot of S_8 with redshift. The results of this analysis, comparing with other data from Planck, is given in Figure 13 below.

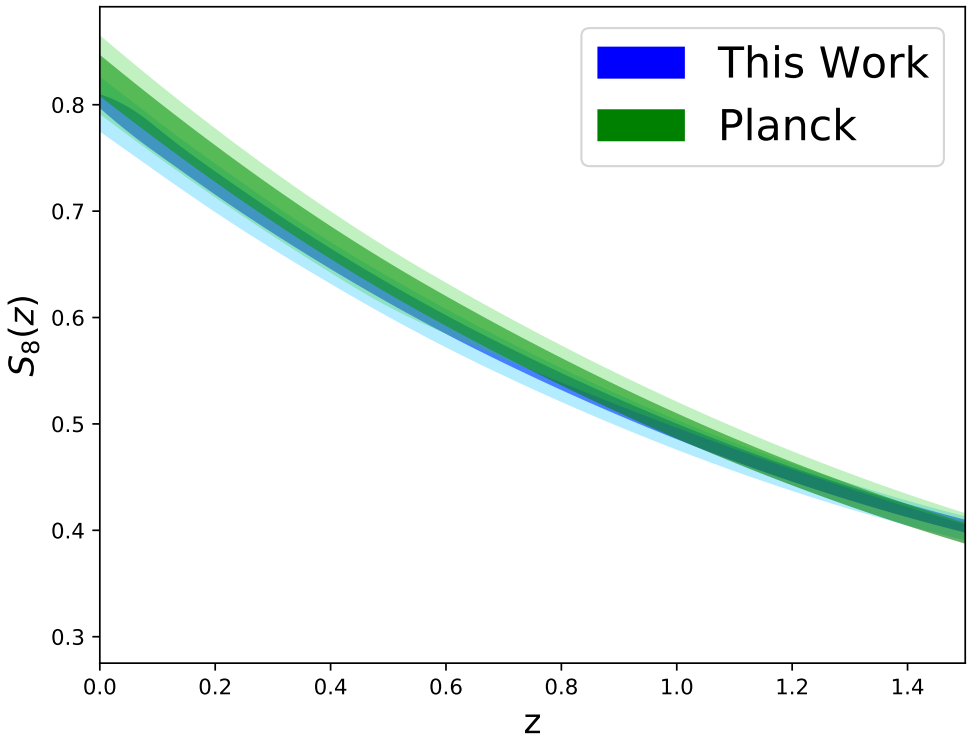

Figure 13: The redshift evolution of the S_8 parameter. Given here is the DDM scenario and also the data obtained by Planck. Confidence bands here represent 1σ and 2σ. We note here the general decrease of the value of S_8 for our decays versus Planck, which gets more and more exaggerated for lower and lower redshifts. We expect this, as our results approach those seen in Figure 11, which is a snapshot of this Figure 13's evolution at $z = 0$. As expected, at high redshift our results are in agreement, as we are using Planck initial conditions.

Concluding this investigation of DDM and structure formation, we have seen how it does not offer a fully satisfactory solution to the σ_8/S_8 tensions. In Figure 13 above we have seen how the redshift-dependent $S_8(z)$ deviates from the ΛCDM growth rate at low redshifts by a small amount. This is currently undetectable with current data. More accurate future measurements of the growth rate as a function of redshift may provide interesting constraints on DDM.

7. Realising Dark Matter Decays Via String Theory

The story, as we have it so far, is not in favour of DDM. It seemingly offers no solution to the H_0 or σ_8/S_8 tensions; any late time data we have is consistent with the ΛCDM model. For an astrophysicist, there seems to be nothing attractive about DDM. But to a string or particle theorist the story may be different.

In recent years, some string theorists have been excited by the possibility of DDM (Agrawal, Obied, and Vafa 2021). In particular, the decay of dark matter may be realised by the coupling of dark matter to a rolling scalar field. Agrawal, Obied, and Vafa (2021) explore this possibility, explicitly in the context of the the effects of such a model on cosmological tensions. We discuss their work at a qualitative level. Their set-up is as follows.

7.1 - Rolling Scalar Fields

We consider a quintessence field: A rolling scalar field in the swampland conjecture motivated by string theory (Vafa 2005). In Agrawal, Obied, and Vafa (2021), they study quintessence models with a specific swampland conjecture: The Distance Conjecture (Ooguri and Vafa 2007). This states that the movement of a slowly-rolling scalar field generates a tower of light states emerge (Grimm, Palti, and Valenzuela 2018). It has been established that quintessence fields cannot interact strongly with baryonic matter (Choudhury, Mondal, and Chatterjee 2018), and as such must reside and interact in the dark sector. Agrawal, Obied, and Vafa (2021) study whether or not we have begun to experience this in the epoch of dark energy becoming dominant in the late-time universe and causing the accelerating expansion of the universe (Riess et al. 1998). This is realised by the coupling of dark energy in the form of this scalar field to dark matter. Such an emergence of states at present times is also claimed to help solve the H_0 tension, increasing the energy density of the universe under this quintessence.

7.2 - What is the Distance Conjecture and What Can It Offer Us?

The distance conjecture is motivated by the observation that light states are seen to emerge when a field travels a distance $\phi >> 1$. We see a mass scale emerge that follows

$$m(\phi) \approx m_0 \times e^{-\tilde{c}\phi} \quad ,$$

where the parameter $\tilde{c}$ is a scaling parameter that can be constrained. This gives a model of dark matter that has an energy density behaving as

$$\rho_{DM} = n_{DM}(a) \times m(\phi) \quad .$$

If we have dark energy as a scalar field in this form, it hence couples to dark matter. This coupling causes dark matter to decay, and so is a realisation of our DDM model.

7.3 - Concluding Quintessence

String theorists are excited by the possibility of detecting the above forms of a rolling scalar field coupled to dark matter. Direct detection of such a coupling would not only help us better understand the nature of dark matter, but also pave the way for string theory to finally resolve its swampland of effective field theories. It provides us, in the context of this project, a way in which to potentially realise our dark matter decays via dark matter actually being coupled to a rolling scalar field, only becoming important at late times. In our current analysis, the coupling of dark energy and dark matter is not investigated. I aim to investigate such models in my next phase of research.

8. Conclusions

The original aim of this project was, at the minimum level, to see if DDM could solve the H_0 tension. It is apparent, and has been since I began work on this project, that DDM offers no such solution. The redshift dilution of radiation relative to matter cannot be overcome, serving only to lower the value of H_0 below the Planck value.

However, we have explored DDM nonetheless and seen several consequences as a result. Characterising our decays by a decay parameter Γ, we have seen how the expansion history is affected by such decays, reproducing the ΛCDM results for $H(z)$, and also with various values of Γ. We have then applied an inverse distance ladder as in Efstathiou (2021) to constrain the expansion history and, importantly, the value of decay parameter, producing $\Gamma = 0.54^{+1.7}_{-0.60}$ kms^{-1}Mpc^{-1}.

We then expanded our scope, investigating the effect of fractional decays, exploring a scenario where only a fraction of the dark matter is subject to decays, whilst the rest is cold. We have seen how this permits very large values of large Γ for small values of the fraction parameter ϵ. This then motivated investigations into structure formation, and a subsequent examination into the σ_8 and S_8 tensions.

We have explored these tensions, and have seen how DDM does indeed offer some level of reconciliation between early time CMB measurements of σ_8 and galaxy lensing measurements offered by the KiDS-1000 team's results. We note how this works for both σ_8 and S_8, and as such not being a result of decreasing the value of Ω_m, used in defining the S_8 parameter. However, the level of reconciliation of datasets when including decays is not large enough to conclude a fully satisfactory solution to the σ_8/S_8 tensions. We then moved away from $z = 0$ to explore the effect of our DDM with the newly defined redshift dependent S_8, exploring the explicit redshift dependence of the overdensity field in our non-ΛCDM universe. We see that our decays lower the value this $S_8(z)$ relative to Planck with decreasing redshift, but importantly still agree to within an acceptable degree of error.

Finally, we qualitatively explored the possibility of a realisation of DDM through dark energy. By examining the distance conjecture in the string swampland, we have seen how a rolling scalar field can produce a tower of light energy states. Identifying this scalar field with dark energy, and coupling this field to our dark matter, we have seen a theoretical possibility of realising DDM via dark energy-dark matter interactions. Importantly, this is a natural result in string theory.

From the early stages of this project it was apparent that the simplest models of DDM could not solve the H_0 tension, but we persisted to examine what else it may offer us. The answer was rather surprising, seeing how DDM had a positive effect on tensions in cosmological structure formation. We examined to what level DDM reconciled CMB and large-scale structure surveys, and saw that it was not enough to conclude a solution to the σ_8/S_8 tensions is provided by our work. We then discussed ways in which our decays could be realised via string theory. Even where (in the likely case) DDM proves to be an non-viable cosmological model, the investigation into late-time changes to ΛCDM offering a solution to cosmological tensions, especially the σ_8 tension, has been enlightening. Other work done in the course of completing this project, (Chen et al. 2021; Davari and Khosravi 2022), is consistent with our own work. These works use various different approaches to our own. They conclude, as we do, that DDM offers no real solution to the main cosmological tensions faced today.

We hope to discover the true nature of dark matter in the future, which would help progress in the ever-expanding literature on this topic, but until such a time we expect various dark matter models to continue to be explored. I hope this work can add some further understanding into what DDM can and cannot offer us.

Appendix A - Deriving the Conservation Equations of Decaying Dark Matter

We can derive the cosmological conservation equations in the context of DDM. General relativity requires the conservation equation

$$\frac{d(\rho a^3)}{da} = -3Pa^2 \ , \tag{14}$$

where P is cosmic pressure, be observed. In general, where we have relativistic decays, $P = w\rho c^2$, with $w = 1/3$. Therefore we have that

$$\frac{d[(\rho_{DM} + \rho_R)a^3]}{da} = -\rho_R a^2 \ . \tag{15}$$

Substituting our form of the dark matter evolution and expanding we have that

$$\frac{d[\rho_{DDM,0}\exp(-\Gamma t) + \rho_{CDM,0}]}{da} + \frac{d[\rho_R a^3]}{da} = -\rho_R a^2 \ , \tag{16}$$

$$-\rho_{DDM,0}\exp(-\Gamma t)\frac{\Gamma}{\dot{a}} + \frac{d\rho_R}{dt}\frac{dt}{da}a^3 + 3a^2\rho_R = -\rho_R a^2 \ . \tag{17}$$

Now collecting and recognising our relation from Equation 5 we have that

$$\boxed{\frac{d\rho_R}{dt} + 4\rho_R\frac{\dot{a}}{a} = \epsilon\Gamma\rho_{DM}} \ , \tag{18}$$

which is our first evolution equation. We also have that

$$\frac{d\rho_{DM}}{dt} = -3\frac{\dot{a}}{a^4}\rho_{DDM,0}\exp(-\Gamma t) - \frac{\Gamma}{a^3}\rho_{DDM,0}\exp(-\Gamma t) - 3\frac{\dot{a}}{a^4}\rho_{CDM,0} \ , \tag{19}$$

such that when we collect terms and recognise our fractions again with Equation 5 we gain

$$\boxed{\frac{d\rho_{DM}}{dt} + 3\rho_{DM}\frac{\dot{a}}{a} = -\epsilon\Gamma\rho_{DM}} \ , \tag{20}$$

as our second evolution equation. Finally, we have an evolution equation for the density of baryons. This is our third equation, given as .

$$\boxed{\frac{d\rho_B}{dt} + 3\rho_B \frac{\dot{a}}{a} = 0}\,. \tag{21}$$

These equations, listed below, are used to evolve the different densities components of the universe from redshift $z = 10$ with ΛCDM priors, as discussed in Section 3. The boxed equations are solved simultaneously for our analysis, with initial cosmic time set at $z = 10$ by the analytical result for a matter dominated universe given by

$$t(z) = \frac{2}{3H_0(1-\Omega_m)^{\frac{1}{2}}} \operatorname{arcsinh}\left[\left(\frac{1-\Omega_m}{\Omega_m}\right)^{\frac{1}{2}} (1+z)^{-\frac{3}{2}}\right]. \tag{22}$$

Appendix B - H_0 and H_0^S

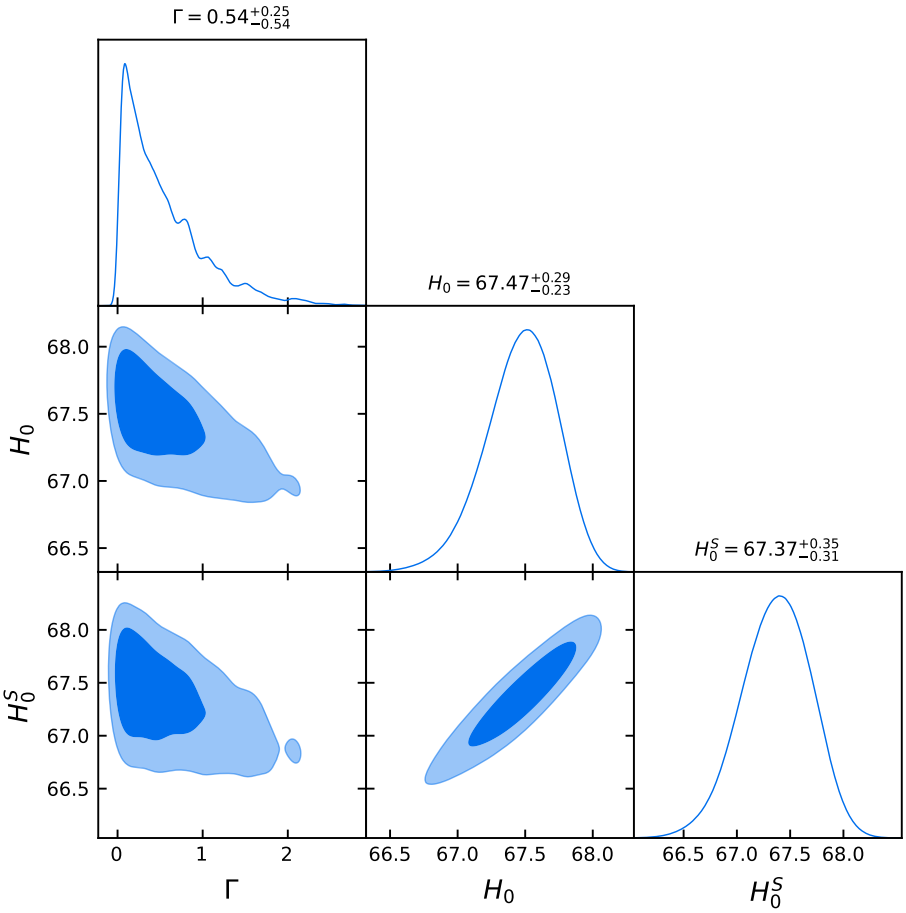

Figure 14: A triangle plot showing two different Hubble parameters. The true Hubble parameter H_0, derived from evolving matter densities in our simulated universe, and the "SH0ES-like" Hubble parameter H_0^S. This parameter is defined as in Efstathiou (2021), where it is derived from constraining the absolute magnitude of SNIa with the pantheon supernovae data. As we are using ΛCDM priors, we recover a value of H_0^S which is consistent with H_0.

We can define an Hubble parameter equivalent to that measured by the SH0ES team via the co-variance matrix of the pantheon supernovae sample C, and the peak absolute magnitude of SNIa, M_B. This follows

$$a_B = \left(\sum_{ij} C_{ij}^{-1} (log_{10} \hat{d}_L(z) - 0.2 m_B(i)) \right) / \sum_{ij} C_{ij}^{-1} \, ,$$

$$H_0^S = 10^{0.2(M_B + 5a_B + 25)} \, .$$

In having used ΛCDM priors, we recover a SH0ES-like H_0^S that is consistent with the Planck value derived from evolving our densities. This is to be expected. In doing this, we have constrained the value of M_B not to the measured SH0ES value of $M_B \approx -19.2$mag, but to -0.2mag lower, and thus have achieved a Planck-like value of the Hubble parameter at $z = 0$ from supernovae data.

References

Abbott, T. et al. (2018). In: *Physical Review D* 98.4. DOI: 10.1103/physrevd.98.043526. URL: https://doi.org/10.1103%2Fphysrevd.98.043526.

Ackerman, L. et al. (2009). In: *Physical Review D* 79.2. DOI: 10.1103/physrevd.79.023519. URL: https://doi.org/10.1103%2Fphysrevd.79.023519.

Agrawal, P., Obied, G., and Vafa, C. (2021). In: *Physical Review D* 103.4. DOI: 10.1103/physrevd.103.043523. URL: https://doi.org/10.1103%2Fphysrevd.103.043523.

Alam, S. et al. (2017). In: *MNRAS* 470.3, pp. 2617–2652. URL: https://doi.org/10.1093%2Fmnras%2Fstx721.

Alcaniz, J. et al. (Jan. 2021). In: *Physics Letters B* 812, p. 136008.

Archidiacono, M. et al. (2019). In: *Journal of Cosmology and Astroparticle Physics* 2019.10, pp. 055–055. URL: https://doi.org/10.1088%2F1475-7516%2F2019%2F10%2F055.

Audren, B. et al. (2014). In: *Journal of Cosmology and Astroparticle Physics* 2014.12, pp. 028–028. URL: https://doi.org/10.1088%2F1475-7516%2F2014%2F12%2F028.

Aylor, K. et al. (2019). In: *The Astrophysical Journal* 874.1, p. 4. URL: https://doi.org/10.3847%2F1538-4357%2Fab0898.

Bernal, J. L., Verde, L., and Riess, A. G. (2016). In: *Journal of Cosmology and Astroparticle Physics* 2016.10, pp. 019–019. URL: https://doi.org/10.1088/1475-7516/2016/10/019.

Blomqvist, M. et al. (2019). In: *Astronomy &amp Astrophysics* 629, A86. DOI: 10.1051/0004-6361/201935641. URL: https://doi.org/10.1051%2F0004-6361%2F201935641.

Bond, J. R., Efstathiou, G., and Silk, J. (1980). In: *Phys. Rev. Lett.* 45. Ed. by M. A. Srednicki, pp. 1980–1984. DOI: 10.1103/PhysRevLett.45.1980.

Buen-Abad, M. A., Emami, R., and Schmaltz, M. (2018). In: *Physical Review D* 98.8. URL: https://doi.org/10.1103%2Fphysrevd.98.083517.

Chen, A. et al. (2021). In: *Physical Review D* 103.12. DOI: 10.1103/physrevd.103.123528. URL: https://doi.org/10.1103%2Fphysrevd.103.123528.

Choudhury, B., Mondal, H., and Chatterjee, D. (Apr. 2018). In: *Pramana* 90, p. 55. DOI: 10.1007/s12043-018-1544-y.

Clark, S. J., Vattis, K., and Koushiappas, S. M. (2021). In: *Physical Review D* 103.4. DOI: 10.1103/physrevd.103.043014. URL: https://doi.org/10.1103%2Fphysrevd.103.043014.

Davari, Z. and Khosravi, N. (2022). In: URL: https://arxiv.org/abs/2203.09439.

Di Valentino, E. et al. (2021a). In: *Astroparticle Physics* 131, p. 102604. URL: https://doi.org/10.1016%2Fj.astropartphys.2021.102604.

Di Valentino, E. et al. (2021b). In: *Classical and Quantum Gravity* 38.15, p. 153001. DOI: 10.1088/1361-6382/ac086d. URL: https://doi.org/10.1088%2F1361-6382%2Fac086d.

Efstathiou, G. (July 2020). In: arXiv: 2007.10716 [astro-ph.CO].

Efstathiou, G. (2021). In: *Monthly Notices of the Royal Astronomical Society* 505.3, pp. 3866–3872. DOI: 10.1093/mnras/stab1588. URL: https://doi.org/10.1093%2Fmnras%2Fstab1588.

Efstathiou, G. and Gratton, S. (2020). In: *Monthly Notices of the Royal Astronomical Society: Letters* 496.1, pp. L91–L95. DOI: 10.1093/mnrasl/slaa093. URL: https://doi.org/10.1093%2Fmnrasl%2Fslaa093.

Enqvist, K. et al. (2020). In: *Journal of Cosmology and Astroparticle Physics* 2020.04, pp. 015–015. DOI: 10.1088/1475-7516/2020/04/015. URL: https://doi.org/10.1088%2F1475-7516%2F2020%2F04%2F015.

Feroz, F. and Hobson, M. P. (2008). In: *MNRAS* 384.2, 449–463. URL: http://dx.doi.org/10.1111/j.1365-2966.2007.12353.x.

Freedman, W. L. (2021). In: *The Astrophysical Journal* 919.1, p. 16. DOI: 10.3847/1538-4357/ac0e95. URL: https://doi.org/10.3847%2F1538-4357%2Fac0e95.

Freedman, W. L. et al. (2020). In: *The Astrophysical Journal* 891.1, p. 57. DOI: 10.3847/1538-4357/ab7339. URL: https://doi.org/10.3847%2F1538-4357%2Fab7339.

García-García, C. et al. (2021). In: *Journal of Cosmology and Astroparticle Physics* 2021. URL: https://doi.org/10.1088%2F1475-7516%2F2021%2F10%2F030.

Grimm, T. W., Palti, E., and Valenzuela, I. (2018). In: *Journal of High Energy Physics* 2018.8. URL: https://doi.org/10.1007%2Fjhep08%282018%29143.

Hamuy, M. et al. (2006). In: *Publications of the Astronomical Society of the Pacific* 118.839, pp. 2–20. DOI: 10.1086/500228. URL: https://doi.org/10.1086/500228.

Heavens, A., Jimenez, R., and Verde, L. (2014). In: *Physical Review Letters* 113.24. URL: https://doi.org/10.1103%2Fphysrevlett.113.241302.
Heymans, C. et al. (2021). In: *Astronomy &amp Astrophysics* 646, A140. URL: https://doi.org/10.1051%2F0004-6361%2F202039063.
Ichiki, K., Oguri, M., and Takahashi, K. (2004). In: *Physical Review Letters* 93.7. DOI: 10.1103/physrevlett.93.071302. URL: https://doi.org/10.1103%2Fphysrevlett.93.071302.
Krisciunas, K. et al. (2017). In: *The Astronomical Journal* 154.5, p. 211. DOI: 10.3847/1538-3881/aa8df0. URL: https://doi.org/10.3847%2F1538-3881%2Faa8df0.
Lemos, P. et al. (2018). In: *Monthly Notices of the Royal Astronomical Society* 483.4, pp. 4803–4810. DOI: 10.1093/mnras/sty3082. URL: https://doi.org/10.1093.
Lewis, A. (2019). In: arXiv: 1910.13970 [astro-ph.IM]. URL: https://getdist.readthedocs.io.
Lin, M.-X. et al. (2019). In: *Physical Review D* 100.6. DOI: 10.1103/physrevd.100.063542. URL: https://doi.org/10.1103%2Fphysrevd.100.063542.
Meszaros, P. (Dec. 1974). In: 37.2, pp. 225–228.
Ooguri, H. and Vafa, C. (2007). In: *Nuclear Physics B* 766.1-3, pp. 21–33. URL: https://doi.org/10.1016%2Fj.nuclphysb.2006.10.033.
Planck collaboration et al. (2018). In: *Astronomy &amp Astrophysics* 641, A6. DOI: 10.1051/0004-6361/201833910. URL: https://doi.org/10.1051%2F0004-6361%2F201833910.
Rameez, M. and Sarkar, S. (2021). In: *Classical and Quantum Gravity* 38.15, p. 154005. DOI: 10.1088/1361-6382/ac0f39. URL: https://doi.org/10.1088/1361-6382/ac0f39.
Riess, A. G. et al. (1998). In: *The Astronomical Journal* 116.3, pp. 1009–1038. URL: https://doi.org/10.1086%2F300499.
Riess, A. G. et al. (Dec. 2021). In: arXiv: 2112.04510 [astro-ph.CO].
Sainte Agathe, V. de et al. (2019). In: *Astronomy &amp Astrophysics* 629, A85. DOI: 10.1051/0004-6361/201935638. URL: https://doi.org/10.1051%2F0004-6361%2F201935638.
Scolnic, D. M. et al. (2018). In: *The Astrophysical Journal* 859.2, p. 101. DOI: 10.3847/1538-4357/aab9bb. URL: https://doi.org/10.3847%2F1538-4357%2Faab9bb.
Scolnic, D. et al. (2021). In: DOI: 10.48550/ARXIV.2112.03863. URL: https://arxiv.org/abs/2112.03863.
Silva, W. da, Gimenes, H., and Silva, R. (2019). In: *Astroparticle Physics* 105, pp. 37–43. URL: https://doi.org/10.1016%2Fj.astropartphys.2018.10.002.
Tröster, T. et al. (2020). In: *Astronomy &amp Astrophysics* 633, p. L10. DOI: 10.1051/0004-6361/201936772. URL: https://doi.org/10.1051%2F0004-6361%2F201936772.
Vafa, C. (2005). In: URL: https://arxiv.org/abs/hep-th/0509212.
Vagnozzi, S. (2021). In:
Vattis, K., Koushiappas, S. M., and Loeb, A. (2019). In: *Physical Review D* 99.12. DOI: 10.1103/physrevd.99.121302. URL: https://doi.org/10.1103%2Fphysrevd.99.121302.
Weinberg, S. (2008). Cambridge University Press.
Zhao, C. et al. (2022). In: *Monthly Notices of the Royal Astronomical Society* 511.4, pp. 5492–5524. DOI: 10.1093/mnras/stac390. URL: https://doi.org/10.1093%2Fmnras%2Fstac390.

Acknowledgements

I would first and foremost like to thank Professor George Efstathiou for helping and supervising me on every stage of this project. Your insights and input have been invaluable, and I feel incredibly lucky to have done this work under your supervision. I'd also like to thank Professor Anthony Challinor and Dr Alexandra Amon for invaluable feedback on my practise presentation and for talking cosmology with me more generally. I'd also like to thank my mum Sharon, dad Jason and sister Charlotte for reminding me to walk away from the laptop every once in a while, and my dog Chester for letting me walk him whenever code wouldn't work. I'd also like to thank my friends Kypros, Luis, Nick, James, Rachael, Tim, Matthew, Joe, Joseph and Euan for being there for me throughout the past year. And, of course, Abbie. For everything.